Soft Matter

PAPER

View Article Online
View Journal | View Issue

Cite this: *Soft Matter*, 2026, **22**, 3506

Reconstitution of metabolic reactions within self-assembled, multi-compartment protein vesicles

Jooyong Shin, Webley Woods and Yeongseon Jang *

Artificial cells that reproduce the spatial organization of metabolism offer a powerful platform for understanding and controlling complex biochemical pathways. In this work, we engineer globular protein vesicles (GPVs) by exhibiting octopine dehydrogenase (ODH), a model monomeric enzyme, on vesicle membranes through the self-assembly of recombinant fusion proteins. The enzymatic GPVs are constructed from two complementary fusion protein building blocks: ODH fused with a glutamic acid-rich leucine zipper (ODH–Z_E) and an elastin-like polypeptide fused with an arginine-rich leucine zipper (Z_R–ELP). The oppositely charged leucine zipper pairs (Z_E and Z_R) form a heterodimer *via* electrostatic interactions, driving vesicle assembly. Because these interactions are sensitive to ionic strength and stoichiometry, we investigate the effects of salt concentration and molar ratio on self-assembly behavior and vesicle morphology. Enzymatic assays show that ODH displayed on GPVs exhibits enhanced stability and sustained catalytic activity compared to the free enzyme. To recapitulate a two-step enzyme cascade representing the terminal steps of glycolysis and anaerobic fermentation observed in marine invertebrates, we created a hierarchical multicompartment architecture consisting of nanoscale ODH-displaying vesicles (~500 nm in diameter) encapsulated within giant GPVs (tens of micrometers). We further engineered co-encapsulation and nested configurations to control pyruvate generation and transport across compartments. Fluorescence-based monitoring of NADH consumption reveals that these architectures produce distinct reaction kinetics, underscoring the role of spatial organization in modulating enzymatic behavior. Together, these results highlight the potential of GPVs as customizable platforms for rebuilding metabolic processes within artificial cell-like compartments.

Received 24th February 2026,
Accepted 10th April 2026

DOI: 10.1039/d6sm00163g

rsc.li/soft-matter-journal

Introduction

Cells are fundamental units of life that organize complex biochemical processes in highly controlled ways to sustain vital functions.[1] To utilize specific cellular functions, researchers have developed artificial cells, which are engineered particles that mimic the structure and function of living cells, offering a powerful platform to study complex biological processes and enable advanced biological applications.[2,3] Various compartmental systems have been developed as artificial cell models, including giant unilamellar vesicles (GUVs)[4] or coacervate droplets.[5] These compartmentalized systems provide simplified and tunable environments for reconstructing cell-like functions, and have been utilized to study spatial organization-mediated enzymatic reactions.[6] Artificial cells aim to replicate several key cellular activities, including signal sensing,[7] cell–cell communication,[8,9] and metabolism,[10] to provide insights into fundamental biological functions.

Among these functions, metabolism is an important biological process, as it provides the energy required to sustain other cellular activities.[11] Mimicking metabolic pathways within artificial cells has emerged as a promising strategy to replicate complex biological reactions for biotechnology applications such as biocatalysis[12] and artificial photosynthetic metabolism.[13] By mimicking these pathways in simplified, controllable environments, researchers can better understand the fundamental principles of metabolism and engineer synthetic systems with tailored biochemical outputs.[14] One of the important aspects of metabolism is its spatial organization. Numerous enzymatic reactions occur at or near biological membranes, where substrate concentrations are enriched and reaction kinetics are tightly regulated.[15] Here, peripheral membrane proteins play a critical role, as they are located at the membranes to localize enzymatic activity, facilitate substrate channeling, and enable spatiotemporal control of material flux.[16,17] Mimicking this membrane-associated architecture in artificial cells not only enhances reaction efficiency but also incorporates the organizational complexity of living cells into synthetic systems. Therefore, integrating peripheral membrane proteins into artificial membranes is essential for advancing the functional complexity of synthetic metabolic networks.

Traditional strategies for localizing water-soluble enzymes to synthetic membranes often rely on chemical conjugation methods.[18,19] For example, proteinosomes, which are typically

Department of Chemical Engineering, University of Florida, 1006 Center Drive, Gainesville, Florida, 32611, USA. E-mail: y.jang@ufl.edu

assembled from protein–polymer conjugates, have been widely explored for enzyme localization and protocell construction.[20,21] While these approaches have enabled important advances in synthetic cell development, chemical conjugation strategies can, in some cases, influence enzyme activity due to conformational changes or nonspecific modification of active sites.[22–25] In addition, the use of organic solvents or reactive linkers during conjugation can compromise protein stability and biocompatibility.[26–28] These limitations have motivated the development of alternative strategies that enable membrane association under mild aqueous conditions, such as the use of genetically encoded affinity domains or self-assembling fusion proteins, to better preserve enzyme function and replicate the dynamic and reversible nature of peripheral membrane proteins in living systems.[29,30]

Globular protein vesicles (GPVs) are self-assembled vesicles, which consist of two recombinant fusion protein building blocks: globular proteins which are fused with a glutamic acid-rich leucine zipper (globule–Z_E) and elastin-like polypeptide (ELP) which are fused with an arginine-rich leucine zipper (Z_R–ELP).[31–33] The Z_E/Z_R pair exhibits high binding affinity, forming a fusion protein complex (globule–Z_E/Z_R–ELP).[34] ELP domains show lower critical solution temperature (LCST) behavior, becoming amphiphilic above the transition temperature and self-assembling into vesicles. By leveraging recombinant technology, the globule domain can be replaced with functional enzymes, which allows the formation of enzyme-displaying protein vesicles without the use of chemical conjugation or organic solvents. The GPV platform has mainly been developed using model globular proteins, such as fluorescent proteins,[35] sensory domains,[36] and antigen proteins,[37] to establish vesicle formation and introduce specific functionalities. Dautel *et al.* also employed several enzymes as model globular domains and established the design rules for GPV self-assembly.[38] However, the use of enzyme-displaying GPVs to reconstitute metabolic pathways within hierarchical multicompartment architectures has not yet been explored.

In this work, we used a fusion protein, ODH–Z_E, where octopine dehydrogenase (ODH) is fused with a glutamic acid-rich leucine zipper (Z_E) to form enzyme-incorporated vesicles. ODH is a monomeric enzyme and plays a key role in anaerobic metabolic pathways under hypoxic conditions, enabling marine invertebrates to produce energy efficiently during anaerobic bursts of activity, such as sudden escapes from predators.[39] Upon coupling with Z_R–ELP, ODH self-assembles into vesicular structures under aqueous conditions (Fig. 1).

This design approach generates self-assembled, multicompartment protein vesicles that encapsulate enzymatic sub-vesicles, enabling biomimetic functions of artificial organelles or compartmentalized bioreactors. To illustrate this capability, we co-encapsulated pyruvate kinase (PK), an enzyme that transfers a phosphate group from phosphoenolpyruvate (PEP) to adenosine diphosphate (ADP) to produce adenosine triphosphate (ATP),

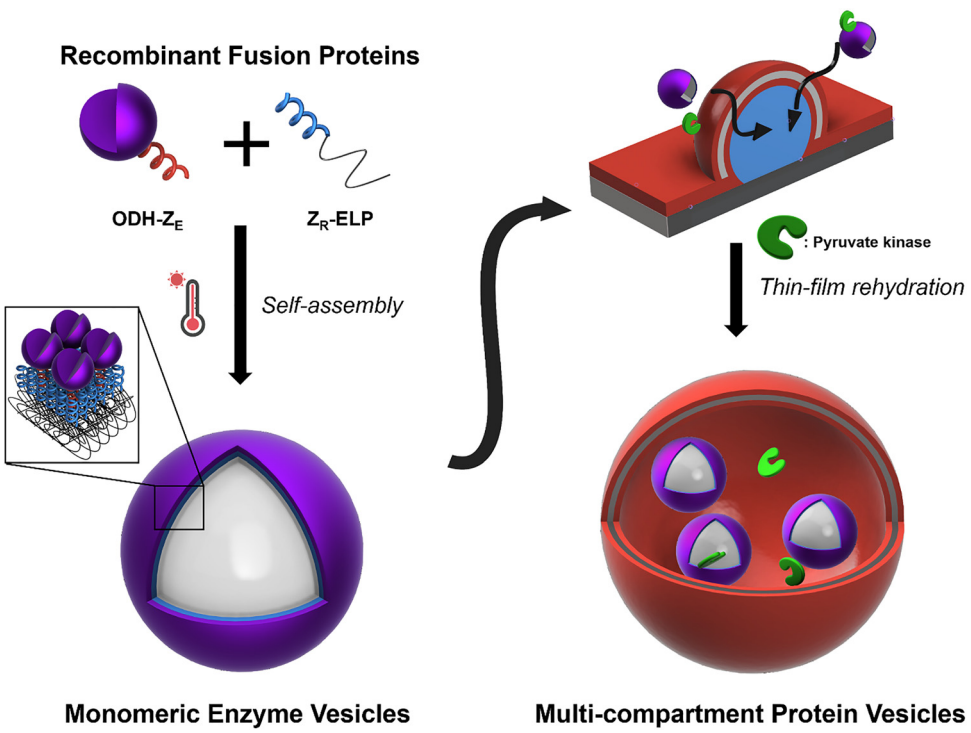

Fig. 1 Schematic overview of the two-step self-assembly process used to generate multicompartment protein vesicles. Globular proteins fused to Z_E (ODH–Z_E or mCherry–Z_E) are mixed with complementary Z_R–ELP to drive temperature-triggered vesicle formation. Small enzymatic vesicles form first from ODH–Z_E/Z_R–ELP, while giant scaffold vesicles form from mCherry–Z_E/Z_R–ELP. Upon mixing these pre-assembled compartments in thin film hydration, giant mCherry-based vesicles encapsulate multiple smaller ODH-based enzymatic vesicles, yielding hierarchical, multicompartment protein vesicles capable of colocalizing enzymes and substrates.

together with ODH-displaying vesicles within GPVs. This multicompartmentalized GPV system in combination with ODH exhibition recapitulates key steps of glycolysis and anaerobic metabolism. By organizing enzyme cascade reactions within multicompartment GPVs and tuning enzyme density at the membrane interface, this work highlights the potential of GPVs as a platform for constructing artificial cells.

Experimental section

Materials

In this work three types of recombinant fusion proteins, Z_R–ELP, mCherry–Z_E, and ODH–Z_E, were used. Z_R–ELP is composed of an arginine-rich leucine zipper (Z_R) genetically fused with elastin-like polypeptide (ELP, $[(VPGVG)_2(VPGFG)(VPGVG)_2]_5$). Globular protein mCherry and octopine dehydrogenase (ODH) are fused with a glutamic acid-rich leucine zipper (Z_E). Pyruvate kinase from rabbit muscle (type III, 350–600 units per mg), adenosine 5′-diphosphate sodium salt (ADP), NADH disodium salt, sodium pyruvate and phsphoenol–pyruvate were purchased from Sigma Aldrich. HisPur Ni-NTA Resin and L-arginine were purchased from ThermoFisher. Tris-glycine plus wedge well gel was purchased from Invitrogen. Rhodamine B (octadecyl ester perchlorate) (RhoB–OEP) was purchased from Chemodex.

Protein expression and purification

The preparation procedures for plasmids for mCherry–Z_E and Z_R–ELP (pQE60-mCherry–Z_E, and pQE60-His6Z_E/Z_R–ELP) are described in previous works.[31] Plasmids for ODH–Z_E (pQE60-ODH–Z_E) were constructed using recombinant techniques. Gene fragments of ODH–Z_E were purchased from Plasmidsaurus and ligated into the HindIII restriction site of the pQE60 vector. All plasmids were transformed into *Escherichia coli* BL21 cells for protein expression. Cultures were grown at 37 °C in LB broth supplemented with ampicillin (200 mg L^{-1}) and chloramphenicol (32 mg L^{-1}). Protein expression was induced by adding 1.0 mM isopropyl β-D-thiogalactoside (IPTG) when the culture reached an optical density at 600 nm of 0.8–1.0. After 5 h of induction at 37 °C, cells were harvested by centrifugation at 4000 × *g* for 30 min. Z_R–ELP was purified under denaturing conditions using buffers containing 8 M urea, 10 mM Tris, and 100 mM Na_2HPO_4 (pH 8 for lysis buffer and pH 6.3 for wash buffer). Cell lysates containing both co-expressed His_6–Z_E and Z_R–ELP were incubated with Ni–NTA resin for 1 h, followed by washing. Z_R–ELP was then eluted from a 6 M guanidine hydrochloride buffer (pH 8), which detached Z_R–ELP from His_6–Z_E. Purified proteins were dialyzed into deionized water. ODH–Z_E and mCherry–Z_E were purified under native conditions using buffers containing 50 mM Na_2HPO_4, 300 mM NaCl, and imidazole at concentrations of 10 mM (lysis), 20 mM (wash), and 250 mM (elution). The final purified proteins were dialyzed into 1× PBS.

Circular dichroism spectroscopy of ODH–Z_E

Far-UV circular dichroism (CD) spectra of the ODH–Z_E fusion proteins were recorded on a Chirascan V100 spectrometer (applied photophysics, Surrey, UK). ODH–Z_E was diluted to a final concentration of 0.2 mg mL^{-1} in DI water. Measurements were performed using a quartz cuvette with a path length of 0.1 cm at 25 °C. Spectra were collected over the range of 180–260 nm with a step size of 1 nm, and an acquisition time of 1 s per point. A buffer-only spectrum recorded under identical conditions was subtracted from the protein spectrum to remove background contributions. The CD signal, initially obtained in millidegrees (mdeg), was converted to mean residue ellipticity, $[\theta]$ (deg cm^2 $dmol^{-1}$), using the molecular weight of ODH–Z_E, the cuvette path length (0.1 cm) and the protein concentration (0.2 mg mL^{-1}).

GPV formation by self-assembly

GPVs are prepared by mixing fusion proteins (ODH–Z_E and Z_R–ELP or mCherry–Z_E and Z_R–ELP) in a specific ratio (from 0.05 to 0.2) to achieve a final fixed concentration of 60 μM of Z_R–ELP. All Z_R–ELP protein is dissolved in 18 MΩ Milli-Q water, and all ODH–Z_E and mCherry–Z_E is dissolved in 1X phosphate-buffered saline (PBS). The salt concentration was adjusted by adding 10X PBS. All solutions were mixed by pipet and incubated for 15 min on ice. The fusion protein mixtures were then incubated at 25 °C for 1 h in a temperature-controlled digital incubator (H2200-HC, Benchmark Scientific).

Enzymatic activity assay

The enzymatic activity of ODH in both soluble and vesicle-incorporated forms was measured by monitoring the decrease in NADH fluorescence (excitation = 340 nm, emission = 460 nm) in the presence of arginine and pyruvate. Reactions were carried out in a total volume of 200 μL in a 96-well clear bottom plate using a microplate reader (BioTek, Synergy H1) at 25 °C. Standard substrate conditions were 0.16 mM NADH, 3 mM pyruvate, and 5.5 mM arginine and excess substrate conditions were 16 mM NADH, 300 mM pyruvate, and 550 mM arginine. For long-term measurement, mineral oil was layered on the top of each well to prevent the evaporation and fluorescence signals were recorded from the bottom of the wells.

Characterization of GPVs

Self-assembled vesicles were characterized *via* optical microscopy, dynamic light scattering (DLS) and transmission electron microscopy (TEM). Bright-field images were obtained using a microscope (LSM 700, Carl Zeiss), and vesicle size distribution was determined using a DLS (Zetasizer Nano ZS, Malvern Instruments). For TEM analysis, vesicles or coacervate samples were loaded onto the carbon-film coated TEM grid (300 MESH, Electron Microscopy Sciences) and left to settle for 10 min at room temperature and negatively stained with 0.5% phosphotungstic acid (PTA). The staining agent was removed *via* filter paper and the grid was washed twice using Milli-Q water followed by drying for 24 h. Membrane fluidity was measured using fluorescence recovery after photobleaching (FRAP) on mCherry–GPVs. FRAP experiments were performed on a LSM 800 (Carl Zeiss). A small circular region of interest (ROI) 0.3 μm on the vesicle membrane was selected for

bleaching, along with a non-bleached reference ROI on the same vesicle or in a nearby vesicle and a background ROI outside any fluorescent structures. The selected ROI was photobleached using the laser at high intensity for 1 s. Immediately after bleaching, time-lapse images were acquired for 2 min at low laser power to monitor fluorescence recovery while minimizing additional photobleaching.

Preparation of multi-compartment GPVs

The preparation procedures for multi-compartment GPVs are described in a previous work.[40] Briefly, 2 mM of Z_R–ELP solutions were mixed with 0.1 mM of mCherry–Z_E at 4 °C and placed on the PDMS well. After evaporation of the solvent at 37 °C to make a film, the protein thin film was immersed in hydration solutions. For the co-encapsulation model, hydration solutions included ODH-displaying vesicles, PK (10.1 unit per mL), ADP (3 mM), NADH (0.16 mM) and L-arginine (5.5 mM) and were incubated for 3 hours. PK and ADP were pre-encapsulated within ODH-displaying vesicles by adding PK during ODH-displaying vesicle assembly for the nested model. In the nested model, the hydration solutions included PK and ADP encapsulated ODH-displaying vesicles, NADH and L-arginine. The collected multi-compartment GPVs were separated from non-encapsulated, small ODH-displaying vesicles by filtration through a 1 μm cell strainer (pluriSelect), where the larger GPVs were retained on the strainer and smaller vesicles passed through.

Results and discussion

Expression and characteristics of the recombinant fusion monomeric enzymes

ODH catalyzes the formation of octopine through reductive condensation of arginine and pyruvate (Fig. 2A). Recombinant ODH–Z_E was expressed in *Escherichia coli* (*E. coli*) and purified by Ni–NTA affinity chromatography (a detailed experimental section is provided in the SI, Fig. 2B). To verify the successful expression of recombinant ODH–Z_E, we performed sodium dodecyl sulfate–polyacrylamide gel electrophoresis (SDS–PAGE). SDS–PAGE analysis of the purified fusion protein showed a predominant band at 44 kDa, corresponding to the expected molecular weight of ODH–Z_E, together with several weaker bands at higher and lower molecular weights (Fig. 2C). Far-UV circular dichroism (CD) spectra confirmed that the ODH–Z_E fusion is well folded and predominantly α-helical (Fig. S1). Deconvolution of the CD spectrum was performed using the ellipticity at 222 nm, a widely used metric for quantifying α-helical contents.[41] This analysis indicated an α-helix content of approximately 45%, which is higher than the ~38% α-helical content reported for wild-type ODH.[42] This increase is consistent with incorporation of the glutamic acid-rich leucine zipper (Z_E), which is predicted to form a coiled-coil α-helix while preserving the overall fold of the ODH catalytic domain. The catalytic activity of purified ODH–Z_E was assessed through microplate readers by measuring the oxidation of nicotinamide adenine dinucleotide (NADH), a key substrate in the ODH catalytic reaction. As NADH is oxidized to NAD^+ during ODH enzymatic reactions, the decrease in NADH fluorescence intensity (excitation: 340 nm, emission: 460 nm)[43] over time indicated that ODH–Z_E has its enzymatic activity upon fusion (Fig. 2D). In addition, the ODH–Z_E fusion proteins shows a turnover number of k_{cat} ($2213 \pm 104\ s^{-1}$), which is comparable to the reported value for wild-type ODH (~$2300\ s^{-1}$ under similar conditions), indicating that fusion to Z_E does not impair catalytic activity.[44,45]

Investigation of self-assembly of ODH–Z_E/Z_R–ELP into enzymatic protein vesicles

When ODH–Z_E and Z_R–ELP are mixed in cold water (molar ratio of ODH–Z_E to Z_R–ELP, $\chi = 0.05$), ODH–Z_E/Z_R–ELP heterodimers and Z_R–ELP homodimers are formed spontaneously due to the

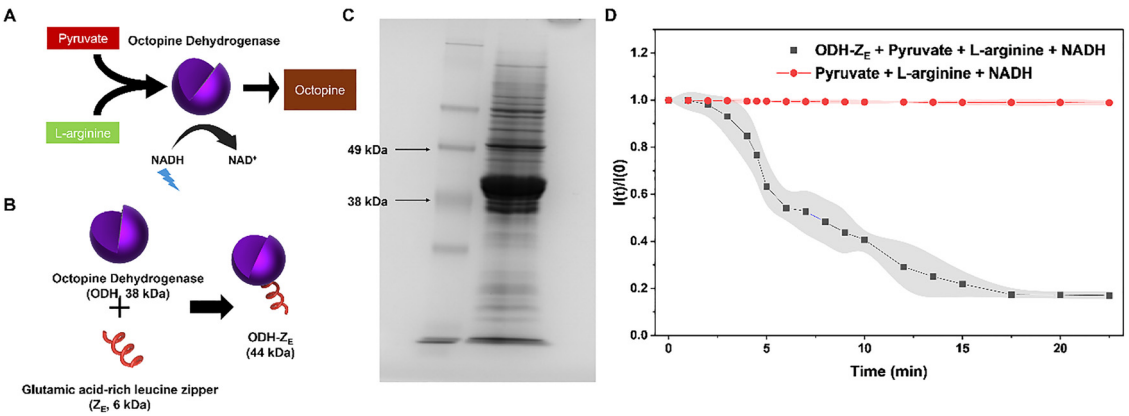

Fig. 2 (A) Schematic image of the octopine dehydrogenase (ODH) reaction converting pyruvate and L-arginine to octopine with the oxidation of NADH to NAD^+. (B) Schematic image of the ODH–Z_E fusion, in which the monomeric ODH domain (purple, 38 kDa) is fused to a glutamic acid-rich leucine zipper (red helix, 6 kDa). (C) SDS–PAGE gel of ODH–Z_E showing a predominant band at the expected molecular weight (44 kDa). (D) NADH fluorescence graph (normalized I/I_0) monitored over time in the presence of ODH–Z_E (black line) and without ODH–Z_E (red line). The decrease in fluorescence with ODH–Z_E confirms that the fusion retains ODH catalytic activity to oxidize NADH. Data represent the mean and standard deviation of each measurement (n = 3). The shaded area indicates the standard deviation.

high binding affinity between complementary leucine zippers (dissociation constant K_d: $Z_E/Z_R \approx 10^{-15}$ M, $Z_R/Z_R \approx 10^{-7}$ M[34]). Our previous work demonstrated that the ELP transition temperature for the current sequence depends on both salt and protein concentrations.[31,32] Under conditions where Z_R–ELP concentrations ranged from 30 to 120 μM in concentrated PBS buffer containing 0.3 M NaCl, the transition temperature was observed between 10 and 20 °C. Salt concentration regulates this self-assembly by altering the hydration and collapse of the ELP domain and by screening electrostatic interactions on the globular headgroup. As salt concentration increases, the protein complexes first condense into protein-rich coacervate droplets and, above a critical salt concentration, undergo a phase transition into membrane-bound vesicles.[32] Therefore, at a room temperature of 25 °C, which is above the transition temperature under our experimental conditions, ODH–Z_E/Z_R–ELP protein complexes can self-assemble into either coacervates or vesicles as a function of salt concentration (Fig. 3A).

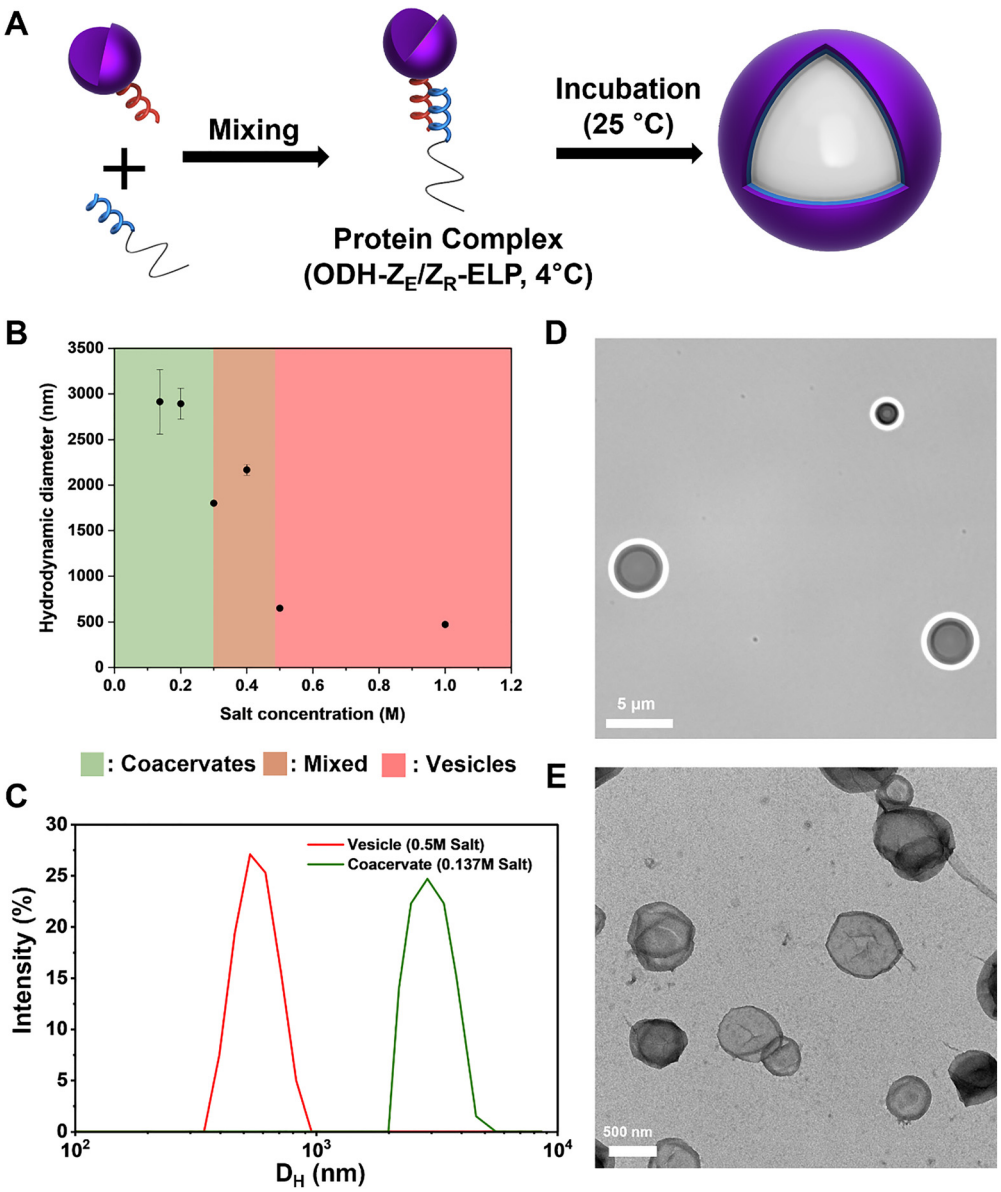

Fig. 3 (A) Scheme of the vesicle formation process driven by the self-assembly of recombinant fusion protein complexes composed of ODH–Z_E and Z_R–ELP. (B) Average hydrodynamic diameter (nm) of ODH–Z_E/Z_R–ELP assemblies as a function of salt concentration, measured by dynamic light scattering (DLS). The green region indicates regimes where coacervates are observed and the red region indicates regimes where vesicles are observed. The brown region is where both coacervates and vesicles are observed. (C) DLS intensity size distributions at low (0.137 M, green) and high (0.5 M, red) salt concentrations, showing a shift from broad, micrometer-scale coacervate droplets to narrow, sub-micrometer scale vesicles. (D) Bright field microscope image of the self-assembled ODH–Z_E/Z_R–ELP coacervate droplets formed at 0.137 M salt concentration, showing micron-sized spherical condensates in solution. (E) Transmission electron microscope (TEM) image of ODH–Z_E/Z_R–ELP vesicles formed at 0.5 M salt concentration, confirming membrane-bound, hollow vesicle structures.

To investigate the salt-dependent structural transition of ODH–Z_E/Z_R–ELP from coacervate droplets to membrane-bound vesicles, dynamic light scattering (DLS) was employed to measure the hydrodynamic diameter and size distribution of the self-assembled structures. In the low salt concentration region, the assemblies showed a large average hydrodynamic diameter with a broad size distribution (Fig. 3B). This behavior is consistent with a coacervate phase composed of liquid–liquid phase-separated droplets that are intrinsically polydisperse, leading to a broad size distribution in DLS.[46] As the salt concentration increased, the mean hydrodynamic diameter decreased and the size distribution narrowed. A significant drop in diameter and size distribution was observed at and above a 0.5 M salt concentration, indicating a transition to smaller, more monodisperse structures. Correspondingly, DLS intensity distributions at 0.137 and 0.5 M salt showed a shift from broad micrometer-scale population to a narrower peak at sub-micrometer diameters (Fig. 3C). Transmission electron microscopy (TEM) and bright-field microscopy were utilized to observe directly the self-assembled structures in different salt concentrations. At 0.137 M salt, liquid–liquid phase separated droplets were observed through bright-field microscopy and TEM (Fig. 3D and Fig. S2 in SI). In contrast, at 0.5 M salt concentration, membrane-bound, hollow vesicle structures were observed (Fig. 3E). Together, the DLS and TEM results demonstrated that the self-assembly behavior of ODH–Z_E/Z_R–ELP depends on the salt concentration and that a critical salt concentration of 0.5 M is required to drive the transition from coacervate droplets to vesicles.

One of the key features of GPV platforms is that the membrane architecture can be engineered between single-layered and double-layered structures depending on the thermal driving force, often expressed as ΔT ($\Delta T = T - T_t$, T: assembly temperature T_t: transition temperature of ELP). Single-layered vesicles are not favorable structures because they are likely to form micelle structures. However, due to the limited mobility and steric hindrance of globular domains, single-layered vesicles are stable and maintain the hollow vesicles structure for 7 days after assembly.[32] Prior studies on mCherry-based GPVs showed that engineering ΔT by varying the ELP concentration governs the formation of single-layered vesicles, with ELP domains oriented toward the lumen, or double-layered vesicles featuring an ELP bilayer centered in the membrane,[32] which in turn modulates membrane permeability.[47]

Guided by prior work, we incorporated the hydrophobic dye rhodamine B octadecyl ester perchlorate (RhoB–OEP) into the ODH-vesicles as a means to confirm the localization of the hydrophobic ELP domain. The ODH-based GPV platform consistently forms single-layered vesicles under conditions (120 μM of Z_R–ELP and 6 μM of mCherry–Z_E) where mCherry–GPVs can form double layer membranes (Fig. S3). Compared to mCherry, ODH has a larger and more bulky size which is likely to induce more steric hinderances. In addition, ODH has more hydrophobic amino acids on the surface than mCherry (Fig. S4). These factors are expected to shift the packing parameter toward values that favor single-layered vesicles rather than double-layered structures, in agreement with previous observations that globular protein size and surface properties strongly influence GPV morphology.[38] A robust single-layered architecture offers distinct advantages for mimicking peripheral or interfacial enzymes that operate on the cell envelope. In ODH-displaying vesicles, the catalytic domains are displayed on the surface side of the membrane, similar to peripheral membrane enzymes that transiently adsorb to membrane surfaces for access of interfacial substrates and often show enhanced activity due to high local concentration.[48] Surface-localized enzyme architectures in proteinosomes and enzyme-decorated vesicles have been shown to support efficient membrane-mediated cascade reactions and interfacial biocatalysis,[49,50] suggesting that single-layered ODH-displaying vesicles could be an attractive platform for constructing membrane-associated metabolic pathways and artificial cell envelopes.

Enzymatic activity in self-assembled structures

Enzyme immobilization on synthetic vesicle membranes has been widely investigated as a strategy to improve catalytic efficiency and stability by concentrating enzymes in a confined area.[19,51] This organization can increase local substrate turnover and reduce diffusion losses. GPVs provide a promising platform for enzyme immobilization, allowing enzymes to be displayed at the vesicle surface. To evaluate the membrane dynamics of GPVs, fluorescence recovery after photobleaching (FRAP) experiments were performed. The GPV membrane, primarily composed of ELP domains, was found to be rigid and exhibited extremely low lateral diffusion. No significant fluorescence recovery was observed within a 2 minute window, which is normally a sufficient time scale for recovery in lipid membranes (Fig. S5). However, previous studies have shown that GPVs still retain lateral mobility over extended timescales, on the order of hours, unlike rigid solid particles that completely lack lateral diffusion.[33] This unique property situates GPVs between liposomes and solid supports. GPVs are more structurally stable than fluid lipid membranes yet retain enough lateral diffusivity to allow dynamic reorganization of membrane components over time. Combined with their ability to encapsulate functional components in the lumen, GPVs offer a versatile and tunable platform for surface enzyme presentation, features that are not readily achievable with solid particles.

To compare the catalytic performance of ODH in different physical states, we evaluated its enzymatic activity in solution and when displayed on vesicles under two substrate conditions: a standard substrate condition (0.16 mM NADH, 3 mM pyruvate, and 5.5 mM arginine) and an excess substrate condition (16 mM NADH, 300 mM pyruvate, and 550 mM arginine). Standard substrate concentrations were chosen to be a few-fold above the reported K_m values for ODH, placing the reaction in a saturating and appropriate condition for initial-rate comparisons between soluble and vesicle bound enzymes.[44,45] We increased all the substrates by 100-fold to maintain saturating conditions over a long time period and to avoid substrate depletion. Under standard substrate levels, the soluble and vesicle-bound ODH showed similar NADH consumption profiles, with only a slight initial decay for the vesicle samples,

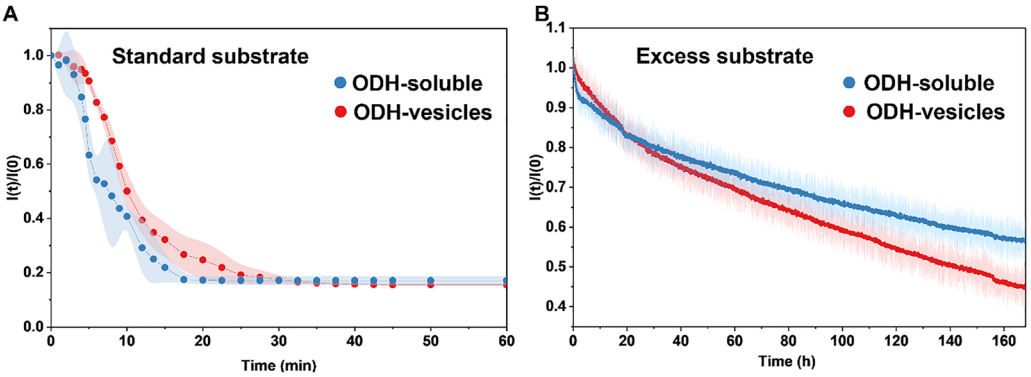

Fig. 4 Comparison of soluble and vesicle-bound ODH activity. (A) NADH fluorescence intensity profile as a function of time for the ODH in solution (blue) and displayed on the vesicle (red) under standard substrate conditions (0.16 mM NADH, 3 mM pyruvate, 5.5 mM L-arginine). (B) NADH fluorescence monitored over an extended period of time (up to 7 days) under excess substrate conditions (16 mM NADH, 300 mM pyruvate, 550 mM L-arginine). The curves represent the mean values, and the shaded regions indicate the standard deviation. Data represent the mean and standard deviation of each measurement (n = 3).

likely indicating limited substrate accessibility to enzyme (Fig. 4A).

However, the difference between these two physical states became clear under excess substrate conditions over an extended time scale. When all substrate concentrations were increased 100-fold and NADH fluorescence was monitored for 7 days, soluble ODH and vesicle-displayed ODH exhibited different behaviors. Soluble ODH showed a rapid initial loss of NADH followed by an early plateau. This indicates a fast burst of activity and subsequent loss or slowdown of enzymatic activity (Fig. 4B). In contrast, vesicle-bound ODH showed a slower but more gradual decay in NADH signal, maintaining enzymatic activity over the full measurement period. After about 24 h, the NADH level in the vesicle sample had dropped below that in the soluble sample, and this difference continued to grow over time. These results suggest that immobilization of ODH on the vesicle membrane preserves enzymatic function and enhances long-term stability, likely because spatial confinement at the membrane reduces enzyme aggregation and protects against deactivation. In addition, membrane immobilization may restrict conformational flexibility, thereby helping to maintain the active structure of the enzyme over extended periods compared to the soluble state.

Control of enzyme density on vesicle membranes

One of the unique advantages of using GPVs is that the number of enzymes displayed on the vesicle surface can be tuned simply by adjusting the molar ratio χ between the two fusion proteins, ODH–Z_E and Z_R–ELP. However, due to the complexity of self-assembly, not all ODH–Z_E are incorporated into vesicles. To quantify the actual incorporation efficiency, we centrifuged the vesicle solution and analyzed the enzyme concentration in the supernatant.

For each molar ratio, we prepared two samples: ODH-displaying vesicles formed by mixing ODH–Z_E with Z_R–ELP, and a soluble ODH–Z_E solution at the same ODH–Z_E concentration used for vesicle assembly but without Z_R–ELP. Upon centrifugation, vesicles pelleted on the bottom while non-incorporated ODH–Z_E remains in the supernatant. By comparing the enzyme activity in the supernatant with that of the soluble ODH–Z_E control, we could analyze how much ODH–Z_E had been incorporated into vesicles (Fig. S6).

Previous studies have demonstrated that ODH binds NADH first, and that hydride transfer from NADH to the enzyme occurs rapidly compared to subsequent steps.[44,45] This results in a sharp initial drop in NADH absorbance, the magnitude of which is proportional to enzyme concentration. We fixed the Z_R–ELP concentration to 60 μM and varied the molar ratio (χ) of ODH–Z_E to Z_R–ELP from 0.05 to 0.2, corresponding to the ODH–ZE concentration from 3 μM to 12 μM. At χ = 0.05, the initial burst amplitude for the supernatant was lower than that of the control, indicating partial removal of the enzyme into the vesicle pellet (Fig. 5A). By comparing the burst phase amplitude of the supernatant (b) to a standard curve generated using known ODH concentrations (a), we estimated how much ODH was incorporated into the vesicle structure. The ratio $\frac{b}{a}$ represents the enzyme that remained unincorporated in the supernatant. Therefore, the enzyme incorporation efficiency was calculated as $\left(1-\frac{b}{a}\right)$. Analysis of three different samples at χ = 0.05, 0.1, and 0.2 showed that all conditions have incorporation efficiencies of ~50% to the fed amounts (Fig. 5B). These results imply that increasing the input ODH–Z_E concentration at fixed Z_R–ELP proportionally increases the number of ODH molecules displayed per vesicle. To further confirm this hypothesis, we measured the average hydrodynamic diameter of ODH-vesicles at each molar ratio (Fig. 5C). Vesicle size decreased as the χ increased, consistent with increased steric hindrance and electrostatic repulsion between densely packed bulky ODH domains favoring higher curvature and smaller vesicles. TEM at a high molar ratio confirmed hollow vesicle structures (Fig. 5D and Fig. S7), indicating that tuning the molar ratio of the two fusion proteins provides a straightforward strategy to

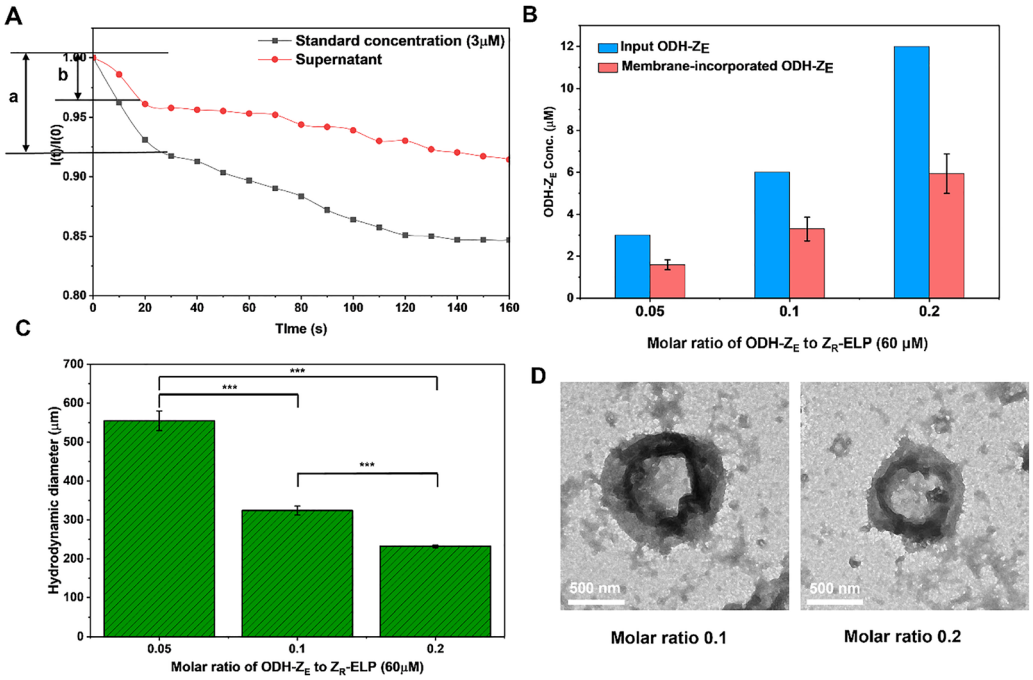

Fig. 5 (A) NADH fluorescence profile for the supernatant after centrifugation of ODH-displaying vesicles prepared at χ = 0.05 (red, Z_R–ELP: 60 μM) and for soluble ODH–Z_E with the same concentration without Z_R–ELP (black). The ratio of reduced burst amplitude (b) in the supernatant to the standard condition (a) reflects removal of the incorporated enzyme into the vesicle pellet. (B) Quantified enzyme incorporation efficiency at different χ = 0.05, 0.1, and 0.2 at fixed Z_R–ELP concentrations of 60 μM. Bars indicate the concentrations of the added ODH–Z_E (blue) and incorporated ODH–Z_E into the membrane (red). (C) Hydrodynamic diameters of the ODH-displaying vesicles measured by DLS as a function of χ, showing a decrease in vesicle size with increasing χ. *** indicate p <0.001. (D) TEM images of ODH-displaying vesicles at high χ of 0.1 (left) and 0.2 (right), confirming hollow vesicle morphology. Scale bars: 500 nm.

engineer the surface density of ODH on GPV membranes without disrupting vesicle architecture.

Multi-compartment protein vesicles for mimicking metabolic pathways

To explore the potential of ODH-displaying vesicles as artificial organelles, we encapsulated them into giant mCherry–GPVs *via* thin film rehydration,[40] thereby reconstructing a multicompartment architecture observed in eukaryotic cells. We then reconstituted two-step enzymatic cascade reactions that mimic the terminal steps of glycolysis and anaerobic pyruvate metabolism by coupling pyruvate kinase (PK) with the ODH-displaying vesicles. PK converts phosphoenol pyruvate (PEP) and adenosine diphosphate (ADP) into pyruvate and adenosine triphosphate (ATP). We designed the resulting pyruvate to subsequently serve as the substrate for the surface-displayed ODH, which then consumes NADH and L-arginine to produce octopine and NAD^+.

In conventional artificial cell platforms such as liposomes, the highly charged PEP is membrane-impermeable and typically requires protein transporters or channels for transmembrane diffusion.[52] However, the GPV membrane is primarily composed of ELP and exhibits temperature-dependent permeability, acting as a molecular gate that regulates transport based on molecular weight. As demonstrated in previous studies, GPV membranes display a temperature-controlled molecular-weight cut off (MWCO) that shifts from ~40 kDa at 25 °C to below 0.4 kDa at 37 °C for single-layered vesicles by utilizing FITC–dextran, which is a widely known membrane-impermeable probe for lipid vesicles.[47] At room temperature, single-layered GPVs have a MWCO of ~40 kDa, so small metabolites such as PEP and pyruvate (<200 Da) are expected to diffuse readily across the GPV membrane.

We further designed two types of multi-compartmental architecture to study the spatial effects of compartmentalization: a co-encapsulation model and a nested model (Fig. 6A). In the co-encapsulation model, pyruvate was generated by PK in the giant GPV lumen and reacted with ODH vesicles encapsulated in the same lumen. In the nested model, pyruvate was generated by encapsulated PK inside ODH-displaying vesicles, requiring the pyruvate to diffuse across the vesicle membrane to react on the exterior facing ODH enzymes. Due to direct substrate access, the co-encapsulation system displayed faster initial reaction kinetics and transitioned to a steady state. However, the nested system showed a delayed onset in NADH consumption due to the time required for pyruvate to diffuse, but it maintained consistent enzymatic kinetics over time (Fig. 6B). After 50 minutes, the nested configuration ultimately showed greater cumulative NADH conversion over the co-encapsulation model, indicating that slower substrate release from the vesicle's interior may prevent excess accumulation of substrates and increase pathways' effectiveness.

Together, these results demonstrate that GPVs provide a versatile platform for programming enzymatic cascades through spatial organization. By tuning whether enzymes and substrates

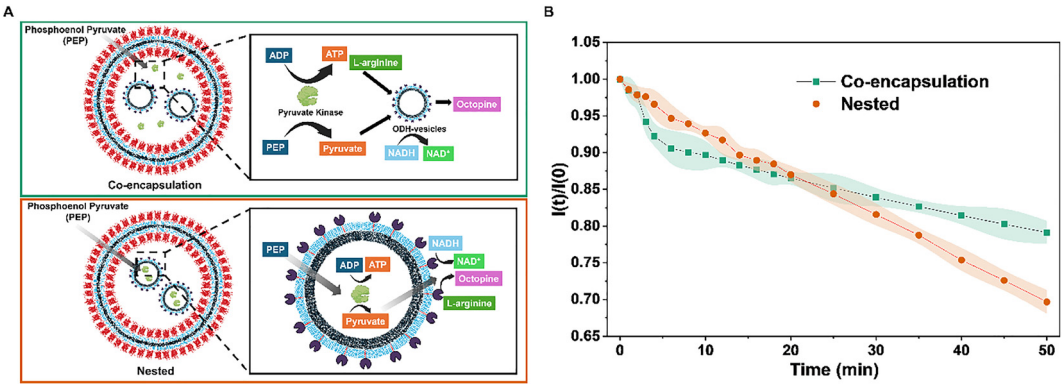

Fig. 6 (A) Schematic image of two structural configurations used to reconstitute a PK → ODH cascade inside giant mCherry GPVs. (Top, green box) Co-encapsulation model: PK and ODH-displaying vesicles are encapsulated together in the giant GPV lumen, allowing pyruvate generated by PK to diffuse toward externally facing ODH vesicles; (bottom, orange box) nested model: PK is encapsulated within the lumen of ODH vesicles, requiring pyruvate produced in the vesicle lumen to diffuse across the membrane to reach the external ODH active sites. (B) NADH fluorescence profile for both the co-encapsulation (green square) and nested (orange circle) models. Co-encapsulation shows a rapid initial decrease in NADH followed by a plateau, whereas the nested model shows a delayed initial NADH consumption but maintains a more sustained rate. Data represent the mean and standard deviation of each measurement (n = 3). The shaded area indicates the standard deviation.

are co-localized in a common lumen or separated by a semi-permeable protein membrane, we can regulate the onset, rate, and efficiency of pathway activity without altering enzyme identity or concentration. This tunability is crucial for building more sophisticated artificial cells, in which spatially organized reaction networks must be coordinated to mimic cellular homeostasis, metabolic channeling, and temporal regulation of biochemical fluxes.

Conclusion

We engineered GPVs to incorporate ODH to mimic metabolic activity within artificial cells. The recombinant fusion protein design enabled enzyme immobilization on vesicle membranes under benign and organic solvent-free conditions, preserving catalytic function. By tuning the salt concentration and molar ratios, we controlled the vesicle formation and enzyme density on the surface. Enzymatic assays demonstrated that vesicle-incorporated ODH maintained long-term catalytic stability compared to soluble forms. Furthermore, by encapsulating ODH vesicles with pyruvate kinase (PK) in multi-compartment GPVs, we reconstituted a two-step enzymatic cascade that mimics natural glycolysis and anaerobic fermentation. Different spatial arrangements, including co-encapsulation and nested models, led to distinct kinetic profiles, highlighting the importance of compartmental organization in regulating reaction dynamics. These results demonstrate that GPVs provide a tunable and modular platform for constructing synthetic metabolic networks and represent a promising approach toward building functionally sophisticated artificial cells. In addition, the GPV platform may be extended to other enzyme classes, including multimeric enzymes and larger protein complexes, provided that their activity is preserved upon fusion. This broader applicability highlights the potential of GPVs as a general platform for reconstructing increasingly complex and spatially organized biochemical pathways in artificial cells.

Conflicts of interest

Ther are no conflicts to declare.

Data availability

All data underlying the results are available as part of the article and in the supplementary information. No additional source data are required.

Supplementary information (SI) contains CD spectrum of fusion proteins, structural characterization of protein assemblies by TEM and fluorescence microscopy, FRAP analysis of vesicle membranes, and experimental method on investigation of enzyme incorporation efficiency. See DOI: https://doi.org/10.1039/d6sm00163g.

Acknowledgements

This research was financially supported by the National Science Foundation (NSF), CAREER Award under grant number 2045313 (CBE). We acknowledge Prof. Julie A. Champion (Georgia Institute of Technology) for providing genetic information encoding recombinant fusion proteins Z_R–ELP and mCherry–Z_E.

References

1 N. A. Yewdall, A. F. Mason and J. C. Van Hest, The hallmarks of living systems: towards creating artificial cells, *Interface Focus*, 2018, **8**(5), 20180023.
2 J. W. Szostak, D. P. Bartel and P. L. Luisi, Synthesizing life, *Nature*, 2001, **409**(6818), 387–390.
3 W. Jiang, Z. Wu, Z. Gao, M. Wan, M. Zhou and C. Mao, *et al.*, Artificial cells: past, present and future, *ACS nano*, 2022, **16**(10), 15705–15733.

4 A. Llopis-Lorente, J. Shao, J. Ventura, B. C. Buddingh, R. Martinez-Manez and J. C. Van Hest, *et al.*, Spatiotemporal communication in artificial cell consortia for dynamic control of DNA nanostructures. ACS Central, *Science*, 2024, **10**(8), 1619–1628.
5 C. Jimenez-Lopez, L. Garcia-Abuin and E. Fernandez-Megia, Dendritic Membranized Coacervate Microdroplets: A Robust Platform for Synthetic-Living Cell Consortia, *J. Am. Chem. Soc.*, 2025, **147**(32), 29457–29467.
6 B. C. Buddingh, A. Llopis-Lorente, L. K. Abdelmohsen and J. C. van Hest, Dynamic spatial and structural organization in artificial cells regulates signal processing by protein scaffolding, *Chem. Sci.*, 2020, **11**(47), 12829–12834.
7 X. Yu, V. Mukwaya, S. Mann and H. Dou, Signal transduction in artificial cells, *Small Methods*, 2023, **7**(12), 2300231.
8 V. Mukwaya, S. Mann and H. Dou, Chemical communication at the synthetic cell/living cell interface, *Commun. Chem.*, 2021, **4**(1), 161.
9 S. Hennig, G. Rödel and K. Ostermann, Artificial cell-cell communication as an emerging tool in synthetic biology applications, *J. Biol. Eng.*, 2015, **9**(1), 13.
10 B. Yang, C. Li, Y. Ren, W. Wang, X. Zhang and X. Han, Construction of the glycolysis metabolic pathway inside an artificial cell for the synthesis of amino acid and its reversible deformation, *J. Am. Chem. Soc.*, 2024, **146**(31), 21847–21858.
11 D. Fell and A. Cornish-Bowden, *Understanding the control of metabolism*, Portland press, London, 1997.
12 H. R. Sikkema, B. F. Gaastra, T. Pols and B. Poolman, Cell fuelling and metabolic energy conservation in synthetic cells, *ChemBioChem*, 2019, **20**(20), 2581–2592.
13 B. Yang, S. Li, W. Mu, Z. Wang and X. Han, Light-harvesting artificial cells containing cyanobacteria for CO2 fixation and further metabolism mimicking, *Small*, 2023, **19**(13), 2201305.
14 M. Kurisu, R. Katayama, Y. Sakuma, T. Kawakatsu, P. Walde and M. Imai, Synthesising a minimal cell with artificial metabolic pathways, *Commun. Chem.*, 2023, **6**(1), 56.
15 X. Lv, Y. Wu, R. Tian, Y. Gu, Y. Liu and J. Li, *et al.*, Synthetic metabolic channel by functional membrane microdomains for compartmentalized flux control, *Metab. Eng.*, 2020, **59**, 106–118.
16 D. M. Boes, A. Godoy-Hernandez and D. G. McMillan, Peripheral membrane proteins: promising therapeutic targets across domains of life, *Membranes*, 2021, **11**(5), 346.
17 K. Moravcevic, C. L. Oxley and M. A. Lemmon, Conditional peripheral membrane proteins: facing up to limited specificity, *Structure*, 2012, **20**(1), 15–27.
18 S. F. Van Dongen, M. Nallani, J. J. Cornelissen, R. J. Nolte and J. C. Van Hest, A three-enzyme cascade reaction through positional assembly of enzymes in a polymersome nanoreactor, *Chem. – Eur. J.*, 2009, **15**(5), 1107–1114.
19 H. Nagata, M. Yoshimoto and P. Walde, Preparation and catalytic properties of carbonic anhydrase conjugated to liposomes through a bis-aryl hydrazone bond, *ACS Omega*, 2023, **8**(21), 18637–18652.
20 X. Huang, A. J. Patil, M. Li and S. Mann, Design and construction of higher-order structure and function in proteinosome-based protocells, *J. Am. Chem. Soc.*, 2014, **136**(25), 9225–9234.
21 A. Joesaar, S. Yang, B. Bögels, A. Van Der Linden, P. Pieters and B. P. Kumar, *et al.*, DNA-based communication in populations of synthetic protocells, *Nat. Nanotechnol.*, 2019, **14**(4), 369–378.
22 W. A. A. Wahab, Review of research progress in immobilization and chemical modification of microbial enzymes and their application, *Microb. Cell Fact.*, 2025, **24**(1), 167.
23 M. S. Robescu and T. Bavaro, A comprehensive guide to enzyme immobilization: All you need to know, *Molecules*, 2025, **30**(4), 939.
24 P. Fernandes and C. C. de Carvalho, Multi-enzyme systems in flow chemistry, *Processes*, 2021, **9**(2), 225.
25 M. M. Elnashar, Immobilized molecules using biomaterials and nanobiotechnology, *J. Biomater. Nanobiotechnol.*, 2010, **1**(1), 61–77.
26 C. Mattos and D. Ringe, Proteins in organic solvents, *Curr. Opin. Struct. Biol.*, 2001, **11**(6), 761–764.
27 R. Sinha and S. K. Khare, Protective role of salt in catalysis and maintaining structure of halophilic proteins against denaturation, *Front. Microbiol.*, 2014, **5**, 165.
28 V. V. Acharya and P. Chaudhuri, Modalities of protein denaturation and nature of denaturants, *Int. J. Pharm. Sci. Rev. Res.*, 2021, **69**(2), 19–24.
29 L. Faltova, A. M. Kuffner, M. Hondele, K. Weis and P. Arosio, Multifunctional protein materials and microreactors using low complexity domains as molecular adhesives, *ACS Nano*, 2018, **12**(10), 9991–9999.
30 A. A. Caparco, D. R. Dautel and J. A. Champion, Protein mediated enzyme immobilization, *Small*, 2022, **18**(19), 2106425.
31 W. M. Park and J. A. Champion, Thermally triggered self-assembly of folded proteins into vesicles, *J. Am. Chem. Soc.*, 2014, **136**(52), 17906–17909.
32 Y. Jang, W. T. Choi, W. T. Heller, Z. Ke, E. R. Wright and J. A. Champion, Engineering globular protein vesicles through tunable self-assembly of recombinant fusion proteins, *Small*, 2017, **13**(36), 1700399.
33 Y. Jang, M.-C. Hsieh, D. Dautel, S. Guo, M. A. Grover and J. A. Champion, Understanding the coacervate-to-vesicle transition of globular fusion proteins to engineer protein vesicle size and membrane heterogeneity, *Biomacromolecules*, 2019, **20**(9), 3494–3503.
34 J. R. Moll, S. B. Ruvinov, I. Pastan and C. Vinson, Designed heterodimerizing leucine zippers with a ranger of pIs and stabilities up to 10− 15 M, *Protein Sci.*, 2001, **10**(3), 649–655.
35 J. Shin, Y. Jia, J. Sampath and Y. Jang, Phase transition of recombinant fusion protein assemblies in macromolecularly crowded conditions, *Mater. Adv.*, 2024, **5**(10), 4200–4208.
36 B. Deb, A. LaVopa, E. McDougal, J. Powers, C. Denard and Y. Jang, Recombinant Fusion Proteins with Embedded Sensing Functions as Versatile Tools for Protocell Development, *Biomacromolecules*, 2024, **26**(1), 279–287.
37 Y. Li, M. R. Rodriguez-Otero and J. A. Champion, Self-assembled protein vesicles as vaccine delivery platform to

enhance antigen-specific immune responses, *Biomaterials*, 2024, **311**, 122666.
38 D. R. Dautel and J. A. Champion, Protein vesicles self-assembled from functional globular proteins with different charge and size, *Biomacromolecules*, 2020, **22**(1), 116–125.
39 M. Grieshaber and G. Gäde, The biological role of octopine in the squid, Loligo vulgaris (Lamarck), *J. Comp. Physiol.*, 1976, **108**(3), 225–232.
40 J. Shin, B. Saha, H. Chung and Y. Jang, Architecting M ulticompartmentalized, Giant Vesicles with Recombinant Fusion Proteins, *Biomacromolecules*, 2024, **25**(9), 6127–6134.
41 S. M. Kelly and N. C. Price, The use of circular dichroism in the investigation of protein structure and function, *Curr. Protein Pept. Sci.*, 2000, **1**(4), 349–384.
42 C. Oriol and A. Olomucki, Spectropolarimetric studies of binary and ternary complexes of octopine dehydrogenase, *Eur. J. Biochem.*, 1972, **29**(2), 288–292.
43 T. M. Cannon, J. L. Lagarto, B. T. Dyer, E. Garcia, D. J. Kelly and N. S. Peters, *et al.*, Characterization of NADH fluorescence properties under one-photon excitation with respect to temperature, pH, and binding to lactate dehydrogenase, *OSA Continuum*, 2021, **4**(5), 1610–1625.
44 M. O. Doublet and A. Olomucki, Investigations on the Kinetic Mechanism of Octopine Dehydrogenase: 1. Steady-State Kinetics, *Eur. J. Biochem.*, 1975, **59**(1), 175–183.
45 M. O. Doublet, A. Olomucki, A. Baici and P. L. Luisi, Investigations on the Kinetic Mechanism of Octopine Dehydrogenase: 2. Location of the Rate-Limiting Step for Enzyme Turnover, *Eur. J. Biochem.*, 1975, **59**(1), 185–191.
46 S. P. Moulik, A. K. Rakshit, A. Pan and B. Naskar, An overview of coacervates: The special disperse state of amphiphilic and polymeric materials in solution, *Colloids Interfaces*, 2022, **6**(3), 45.
47 J. Powers and Y. Jang, Temperature-responsive membrane permeability of recombinant fusion protein vesicles, *Soft Matter*, 2023, **19**(18), 3273–3280.
48 C. D. Radka, Interfacial enzymes enable Gram-positive microbes to eat fatty acids, *Membranes*, 2023, **13**(4), 423.
49 X. Wu, H. Karring, Z. Wang and C. Wu, Protein-cell conjugates as artificial surface display for interfacial biocatalysis, *Chem. Sci.*, 2025, **16**(11), 4892–4899.
50 X. Huang, M. Li and S. Mann, Membrane-mediated cascade reactions by enzyme–polymer proteinosomes, *Chem. Commun.*, 2014, **50**(47), 6278–6280.
51 M. L. Corvo, H. S. Marinho, P. Marcelino, R. M. Lopes, C. A. Vale and C. R. Marques, *et al.*, Superoxide dismutase enzymosomes: Carrier capacity optimization, in vivo behaviour and therapeutic activity, *Pharm. Res.*, 2015, **32**(1), 91–102.
52 A. N. Trementozzi, C. Zhao, H. Smyth, Z. Cui and J. C. Stachowiak, Gap junction-mediated delivery of polymeric macromolecules, *ACS Biomater. Sci. Eng.*, 2022, **8**(4), 1566–1572.

